

Full-scale test of dampers for stay cable vibration mitigation and improvement measures

Haijun Zhou^{*1,2}, Ning Xiang^{1,2a}, Xigui Huang^{1,2b}, Limin Sun^{3c},
Feng Xing^{2d} and Rui Zhou^{1e}

¹*Institute of Urban Smart Transportation & Safety Maintenance, Shenzhen University, Shenzhen 518060, China*

²*Guangdong Provincial Key Laboratory of Durability for Marine Civil Engineering, Shenzhen University, Shenzhen 518060, China*

³*State Key Laboratory for Disaster Reduction in Civil Engineering, Tongji University, Shanghai 200092, China*

(Received February 10, 2018, Revised August 17, 2018, Accepted October 29, 2018)

Abstract. This paper reported test of full-scale cables attached with four types of dampers: viscous damper, passive Magneto-Rheological (MR) damper, friction damper and High Damping Rubber (HDR) damper. The logarithmic decrements of the cable with attached dampers were calculated from free vibration time history. The efficiency ratios of the mean damping ratios of the tested four dampers to theoretical maximum damping ratio were derived, which was very important for practical damper design and parameter optimization. Non-ideal factors affecting damper performance were discussed based on the test results. The effects of concentrated mass and negative stiffness were discussed in detail and compared theoretically. Approximate formulations were derived and verified using numerical solutions. The critical values for non-dimensional concentrated mass coefficient and negative stiffness were identified. Efficiency ratios were approximately 0.6, 0.6, and 0.3 for the viscous damper, passive MR damper and HDR damper, respectively. The efficiency ratio for the friction damper was between 0-1.0. The effects of concentrated mass and negative stiffness on cable damping were positive as both could increase damping ratio; the concentrated mass was more effective than negative stiffness for higher vibration modes.

Keywords: stay cable; damper; damping ratio; negative stiffness; concentrated mass

1. Introduction

Stay cables are vulnerable to environmental excitations (Hikami and Shiraishi 1988). Harmful vibrations can lead to collisions or induce secondary stress for the HDPE sheath near the cable anchorage. Engineering societies have mainly attributed the reported corrosion and failure of

*Corresponding author, Professor, E-mail: haijun@szu.edu.cn

^a Postgraduate Student, E-mail: 2890520030@qq.com

^b Postgraduate Student, E-mail: 847076858@qq.com

^c Professor, E-mail: lmsun@tongji.edu.cn

^d Professor, E-mail: xingf@szu.edu.cn

^e Assistant Professor, E-mail: zhourui@szu.edu.cn

high-strength wires of stay cables with a shorter-than-expected life-span to damage in corrosion protection system.

Throughout the last four decades, bridge engineers have been proposed different measures to suppress these harmful vibrations. One typical countermeasure is to attach the damper near cable anchorage to provide additional damping for the cable (Yamaguchi and Fujino 1998). Different kinds of dampers with varying working mechanisms have been employed to suppress harmful vibrations. Theoretical studies have also been conducted to explore damping effects. Pacheco *et al.* (1993) proposed a “universal design curve” for damper constant optimization. Then, an approximate closed-form solution was further developed by Krenk (2000) and widely applied in engineering practice for optimization of linear viscous damper constant. However, each kind of damper has a specific force–velocity relationship. Non-ideal factors, such as cable bending stiffness (Tabatabai and Mehrabi 2000, Main and Jones 2007), cable sag (Xu and Yu 1998, Krenk 2002), damper supporter flexibility (Xu and Zhou 2007), damper friction threshold (Main and Jones 2002a), and damper internal stiffness (Zhou *et al.* 2014a, b) can affect damping of a cable with attached damper. Addressing these factors precisely by theoretical analysis alone remains challenging, as their effects are combined together. These factors are also difficult to quantify because they are related to boundary conditions or a complex damper/cable working mechanism. As such, testing a full-scale stay cable with damper is crucial to measuring actual damper performance. The ratio of the tested damping ratio to the maximum theoretical damping ratio can be derived from the test; which can then be feedback to optimize damper parameters. This paper reported full-scale cable tests of four typical kinds of dampers. Factors that could affect damper performance, especially those may increase the attainable maximum damping ratio, were addressed theoretically for further damper development.

2. Passive dampers

Different dampers have different working mechanisms. In this paper, four representative kinds of dampers (viscous damper, magnetorheological (MR) damper, friction damper and high damping rubber (HDR) damper) were tested with the full-scale cable.

2.1 Viscous damper

The viscous dampers in this test were jointly developed by Tongji University and Shanghai Materials Research Institute. The ideal damper force is highly dependent on velocity

$$F_d(v) = c|v_d|^{\varepsilon-1}v_d \quad (1)$$

where F_d is the damper force, c is the damping coefficient, ε is an exponent that varies from 0.3-1.95 in engineering practices (Lee and Taylor 2001), and v_d is damper piston velocity. The viscous damper will be similar to a friction damper when $\varepsilon \approx 0$ (Fig. 1).

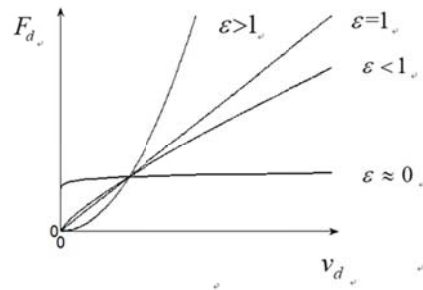


Fig. 1 Schematic force–velocity curve of power–law damper (Main and Jones 2002c)

2.2 MR damper

The tested RD -1005 MR dampers were purchased from Lord Corporation. It is a special type of damper that contains MR fluid as viscous fluid. It is also a controllable damper as the MR fluid greatly increases its apparent viscosity when subjected to a magnetic field (Spencer *et al.* 1997). Although this damper offers the advantage of semi-active control, it can also be used as a passive damper for the sake of simplicity.

2.3 Friction damper

The friction damper in this study was provided by VSL International. It translates kinetic energy into heat by coulomb friction. Compared to the above two dampers with viscous fluid, the friction damper uses solid materials for energy dissipation. The friction force is unrelated to velocity; also due to static friction, the friction has a “fuse” force (amplitude, for cable vibration) to start working.

2.4 HDR damper

The HDR damper in the test was developed in Japan by Sumitomo Rubber Industries. The HDR damper has the advantage of low sensitivity to temperature, and the optimum damping coefficient does not vary depending on the vibration frequency (Nakamura *et al.* 1998). Similar to friction damper, HDR dampers are highly compact and easy to implement as they are also in a solid state and can be modularized in applications (Fig. 2).



Fig. 2 HDR damper pad

3. Full-scale cable test

3.1 Experimental setup and test method

There were three prototype cables tested in three cable factories (Jiangyin Fasten, Shanghai Pujiang and Liuzhou OVM). The test cases were shown in Table 1. The two cables in Jiangyin Fasten and Shanghai Pujiang cable factories were identical. Installation locations of viscous damper, MR damper and friction damper were also the same. The cable parameter and damper location in Liuzhou OVM were different from the above two cables as listed in Table 2. The tested results in Jiangyin Fasten and Shanghai Pujiang cable factories were almost the same, so the test results of the MR damper and friction damper in Jiangyin Fasten cable factory and the viscous damper in Shanghai Pujiang cable factory were reported in this paper for the sake of simplicity.

The instrument setup of the test in Jiangyin Fasten and Shanghai Pujiang cable factories were shown in Fig. 3. There were 6 displacement meters installed at the damper location, $L/8$, $L/2$, $L/4$, $3L/4$, and $7L/8$ in vertical direction. Five vertically oriented accelerometers were placed near the damper location, and at $L/8$, $L/2$, $L/4$, $L/2$; L was cable chord length. One transversely oriented accelerometer was located at $7L/8$. The load cells were connected to viscous and MR dampers in series during the test; however, there was no load cell for the friction damper test. The experimental setup in Liuzhou OVM was simple compared to that of the above two factories. Three displacement meters in vertical direction (at damper location, $L/4$, and $L/2$, respectively) and two accelerometers also in vertical direction (at $L/4$ and $L/2$, respectively) were installed for the HDR damper test in Liuzhou OVM. There was no load cell in series with the tested damper in Liuzhou OVM too.

Table 1 Test cases

Cable factories	Tested dampers
Jiangyin Fasten	Viscous damper
	MR damper
	Friction damper
Shanghai Pujiang	Viscous damper
	MR damper
	Friction damper
Liuzhou OVM	HDR damper

Table 2 Parameters of the full-scale cables

Location	Cable length (m)	Mass (ton)	Tension force (kN)	Cable type (PWS)	Diameter (mm)	Natural frequency (Hz)		
						1 st	2 nd	3 rd
Jiangyin (Shanghai)	215.58	10.61	3955.80	Φ7×151	113	0.658	1.316	1.974
Liuzhou	168.25	4.71	2731	Φ7×85	87	0.928	1.856	2.784

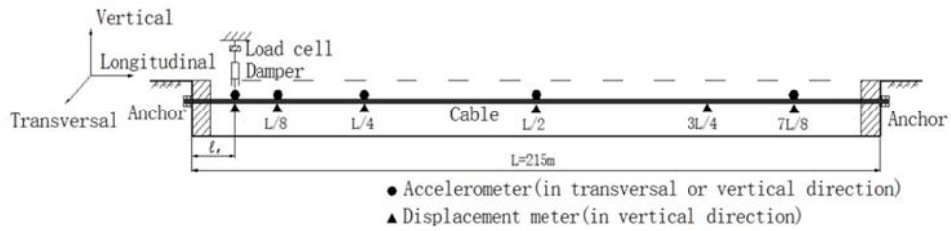


Fig. 3 Experimental setup (Jiangyin and Shanghai)



(a) Full-scale cable (Jiangyin)



(b) Viscous damper (Shanghai)



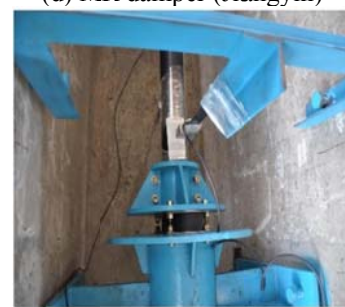
(c) Full-scale cable (Liuzhou)



(d) MR damper (Jiangyin)



(e) Friction damper (Jiangyin)



(f) HDR damper (Liuzhou)

Fig. 4 Full-scale cable test

The tested four types of dampers are shown in Fig. 4. The installation position of viscous damper, MR damper and friction damper was 5.0 m from the anchorage ($l_1/L = 2.32\%$, l_1 is distance from the damper location to the nearest cable end). The two viscous dampers (Fig. 4(b)) were placed on the cable at an angle of 60° to suppress vertical and transversal cable vibrations; while the two MR dampers (Fig. 4(d)) were placed on the cable at an angle of 45° . The voltages applied to the MR dampers ranged from 0.0 V (no voltage applied), 3.0V, 6.0V, 9.0V and 12.0V, respectively (Zhou and Sun 2013). The tested friction damper included four friction pads (Fig. 4(e)), which were attached to the steel plate by high-precision bolts. The friction force could be adjusted by loosening or tightening the bolts (Fig. 4(e)). The damping force of the friction damper was set to 2000N and 2500N (Zhou *et al.* 2006). A pair of HDR dampers was used in the full-scale cable test (Fig. 4(f)). The installation position of HDR dampers was 6.73 m from the cable anchorage ($l_1/L = 4.00\%$).

The full-scale cable could be easily excited by human excitation at the anti-node of the vibration mode shape with the frequency tuned to the cable frequency. The location of human excitation was $L/2$ for the first and the third modes, $L/4$ for the second mode. When the vertical vibration amplitude reached to the designated value, the excitation was stopped and then the cable continued to decay freely. The free decay time history of the vertical vibration was recorded and the logarithmic decrement of the cable δ'_a could be estimated using the following formula (Clough and Penzien 2003)

$$\delta'_a = \frac{1}{b} \ln \left(\frac{A_{a-b/2}}{A_{a+b/2}} \right) \quad (2)$$

where $A_{a-b/2}$, $A_{a+b/2}$ are the double amplitude of the $(a-b/2)^{th}$ and the $(a+b/2)^{th}$ period of oscillation, respectively, and δ'_a denotes the logarithmic decrement corresponding to A_a (i.e., the double amplitude of the a^{th} period). In this paper, the data was processed using $b = 20$ for those cases with dampers and 100~300 for free cable. As the damping value of the cable before/after damper installation is very small, the corresponding modal damping ratio of the cable ξ_a could be estimated (Clough and Penzien 2003)

$$\xi_a \approx \frac{1}{2\pi} \delta'_a \quad (3)$$

3.2 Damping and frequency of free cable

Fig. 5 shows the first mode free vibration decay and the calculated logarithmic decrement of free cable in Shanghai Pujiang cable factory. Table 3 lists the first three mode vibration frequencies using Fast Fourier Transform from free vibration decay of the free cable. The mean logarithmic decrements for the first three modes of free cable were also listed in Table 3. It was found that the tested damping of free cable was very small, about 0.0112 in mean logarithmic decrement value for the first mode, and even lower for the second and the third modes. The internal damping of the

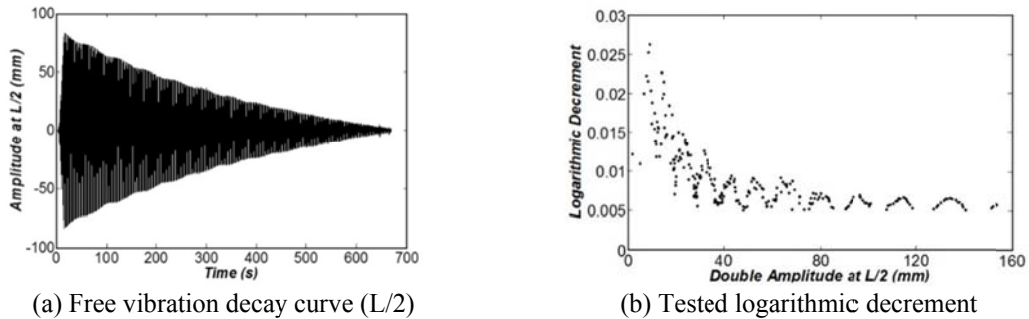


Fig. 5 Test results of the free cable (first mode)

Table 3 Measured frequency and mean logarithmic decrement of the free cable

Mode No.	1 st	2 nd	3 rd
Frequency (Hz)*	0.653 (-0.73%)	1.294 (-1.70%)	1.940(-1.75%)
Logarithmic decrement (Mean value)	0.0112	0.0021	0.0014

*in bracket is the difference between measured and calculated frequency

cable is thus ignored in the following analysis. The measured frequencies of free cable were very close to the predicted ones based on the taut string assumptions (Irvine 1981).

3.3 Tested mechanical behavior of viscous and MR dampers

The force–velocity relations of the viscous damper and MR damper (input voltage of 6.0V) in the first mode of vibration were shown in Figs. 6(a) and 6(b), respectively. Fig. 6(a) showed force–velocity relation of the viscous damper was nonlinear; the force increased much more quickly when the velocity was small. The force–velocity relationship in Fig. 6(a) was also scattered in a particular area, indicating that the viscous damper provided elastic restore force component. Fig. 6(b) showed the force–velocity relationship of the MR damper at an input voltage of 6.0V. The force obviously increased faster than that of the viscous damper at a lower velocity, but the force did not increase when it reached about 2000N. The elastic restore force component also appeared in the force-velocity curve of the MR damper, especially at lower velocities as the force–velocity dots were clustered in a certain area as shown in Fig. 6(b).

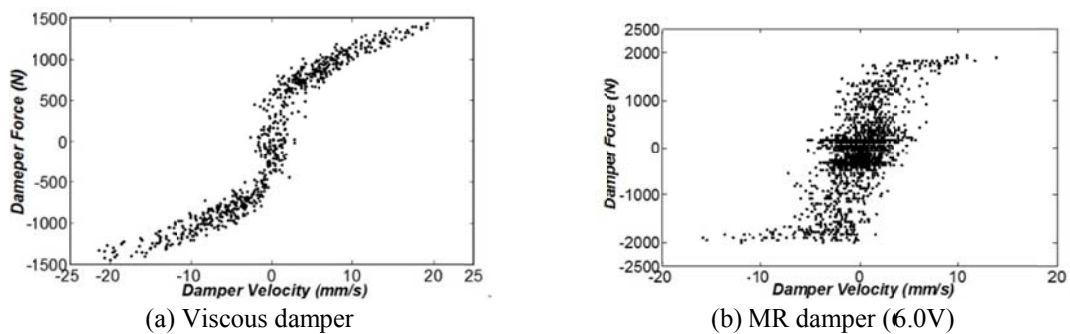


Fig. 6 Tested force–velocity data of damper (first mode)

3.4 Tested logarithmic decrement

Figs. 7-10 showed the tested logarithmic decrement of the cable attached with four different dampers derived from the free decay of the first and the second modes, respectively. Logarithmic decrement values corresponding to double amplitude lower than 10 mm were considered not to be reliable, as the effects of a small gap and friction became significant for small-amplitude vibration.

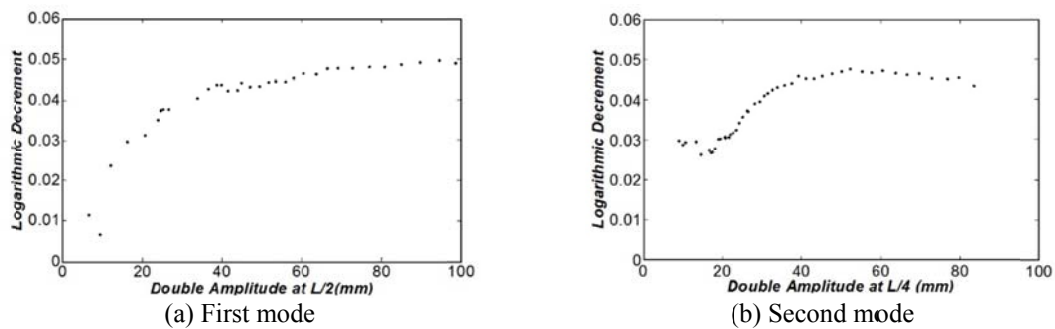


Fig. 7 Tested logarithmic decrement of full-scale cable attached with viscous dampers

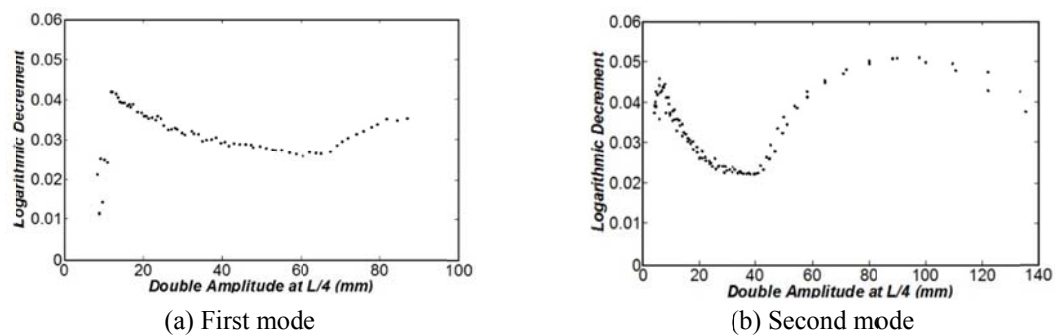


Fig. 8 Tested logarithmic decrement of full-scale cable attached with MR dampers (6.0V)

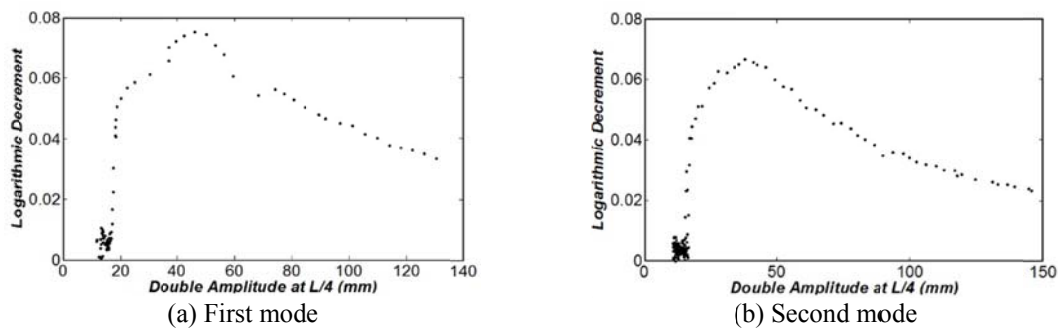


Fig. 9 Tested logarithmic decrement of full-scale cable attached with friction damper

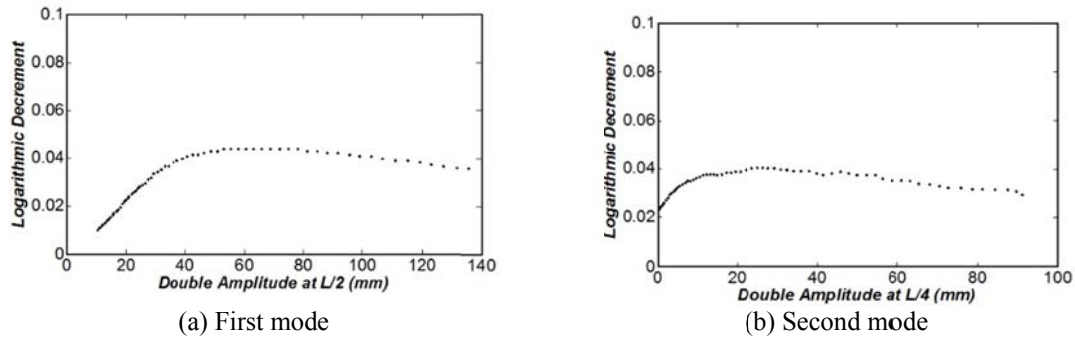


Fig. 10 Tested logarithmic decrement of full-scale cable attached with HDR damper

Fig. 7 showed the logarithmic decrement of the cable attached with viscous dampers for the first mode and the second mode. The logarithmic decrement of the first mode decreased gradually as the amplitude decreased. It reached a maximum of approximately 0.05 when the double amplitude was around 100 mm. The logarithmic decrement of the second mode increased firstly as the amplitude decreased, then reached a maximum value and began decreasing again. The maximum logarithmic decrement of the second mode was about 0.05 when the double amplitude was around 50 mm. It should be noted that similar phenomenon was found for the logarithmic decrement of the third mode in the test.

Fig. 8 depicted the MR-damped cable with 6.0V voltage for the first mode and second mode. The logarithmic decrements of the first mode and the second mode were larger than 0.04 when the double amplitude was around 10mm. The first mode logarithmic decrement decreased to a minimum value and then increased again as the vibration amplitude decreased. The minimum logarithmic decrement of the first mode was approximately 0.03 when the double amplitude was around 70mm. The logarithmic decrement of the second mode decreased firstly as the amplitude increased, then reached a minimum value and began to increase again, eventually reached a maximum value and then once again decreased with increasing amplitude. The minimum logarithmic decrement of the second mode was approximately 0.02 when the double amplitude was around 40 mm. The maximum logarithmic decrement of the second mode was approximately 0.05 when the double amplitude was around 90 mm. It was also found that the logarithmic of the third mode had similar phenomenon.

Fig. 9 showed the tested logarithmic decrement of the cable with an attached friction damper for the first mode and second mode. As amplitude decreased, the logarithmic decrement of the first mode increased firstly and reached a maximum value of approximately 0.075 at double amplitude around 45 mm, then decreased sharply as the amplitude continued decreasing to the “stop” amplitude. This “stop” amplitude corresponded to the static friction force that locked the cable. Then the friction damper did not work, and the rest of the cable vibrated with a damping value the same as that of the free cable. The logarithmic decrement and amplitude curves were similar for the second mode except that the maximum logarithmic decrement of the second mode was approximately 0.07 when the double amplitude was around 40 mm.

The logarithmic decrement of the cable attached with HDR damper (Fig. 10) tended to increase first as the amplitude decreased for the first mode and the second mode, and then the logarithmic decrement decreased as the amplitude decreased. The logarithmic decrement of the first mode reached a maximum of approximately 0.04 when the double amplitude was around 50 mm. The

logarithmic decrement of the second mode was similar to that of the first mode, however, the maximum logarithmic reached a maximum of approximately 0.04 when the double amplitude was around 30 mm.

The above test results indicated the dependence of damping on amplitude due to the effects of nonlinearity (Main and Jones 2002c). It also showed that the tested maximum logarithmic decrement was lower than the theoretical maximum logarithmic decrement. To compare damper performance, the damper efficiency ratio was defined as the mean logarithmic decrement to the maximum theoretical logarithmic decrement. And the attainable maximum theoretical logarithmic decrement δ_{\max} was calculated using the following formula (Krenk 2000)

$$\delta_{\max} \approx 2\pi\xi_{\max} \approx \pi l_1/L \quad (4)$$

Where ξ_{\max} is the maximum theoretical damping ratio of the cable attached with linear damper. The damper efficiency ratio χ was calculated using the following formula (Zhou 2005)

$$\chi = \frac{\delta'_m}{\delta_{\max}} \approx \frac{\delta'_m}{\pi l_1/L} \quad (5)$$

where δ'_m is the measured mean logarithmic decrement of the cable attached with the damper. For the same installation location of viscous damper, MR damper, and friction damper ($l_1/L = 0.023$), δ_{\max} is about 0.072. For the installation location of the HDR damper ($l_1/L = 0.040$), δ_{\max} is about 0.126.

Table 4 Mean logarithmic decrement values and efficiency ratios

Passive dampers	Mode No.	Mean logarithmic decrement value	Efficiency ratio
Viscous damper	1 st	0.045	0.63
	2 nd	0.038	0.53
	3 rd	0.042	0.58
MR damper (6.0V)	1 st	0.043	0.65
	2 nd	0.041	0.57
	3 rd	0.041	0.58
Friction damper	1 st	0.043	(0~1.00)
	2 nd	0.033	(0~0.92)
	3 rd	0.028	(0~0.60)
HDR damper	1 st	0.042	0.33
	2 nd	0.037	0.29
	3 rd	0.034	0.27

Table 4 listed the mean logarithmic decrements of the first three modes of the cable attached with dampers and the corresponding efficiency ratios. The mean logarithmic decrement was larger than 0.03 for most tested cases. The friction damper was an exception because of its unique working mechanism, which will stopped operating when the vibration amplitude was below the “threshold” value. The efficiency ratio was approximately 0.6 for viscous damper and passive MR damper. The HDR damper was inferior to the others with an efficiency ratio of about 0.3; however, it was still acceptable as the mean logarithmic decrement was larger than 0.03 for the first three modes.

The test results show that many non-ideal factors can affect passive damper performance in engineering applications, some of which may reduce damper performance, especially in terms of stiffness observed in the force-velocity relation (Zhou *et al.* 2014a, b). Therefore, some researchers have proposed installing viscous damper with negative stiffness spring to improve damping performance (Chen *et al.* 2015, Zhou and Li 2016, Shi *et al.* 2016). While recent investigation shown that the effects of concentrated mass exert similar damping improvement effects as negative stiffness (Lazar *et al.* 2016, Lu *et al.* 2017, Zhou *et al.* 2018). The effects of the two factors will be discussed in the following section.

4. Effects of negative stiffness and concentrated mass

4.1 Dynamic formulation

Fig. 11 shows a taut cable with an attached damper with a concentrated mass and negative stiffness spring. The cable tension force is T and the mass per unit length of the cable is m . M is the concentrated mass and $l_2 = L - l_1$, $-k$ is the negative stiffness and $k > 0$, the damper is assumed as linear with damping coefficient c . The effects of cable sag are small for most of cables and therefore were ignored.

The free vibration equation of the cable system in the transverse direction can be expressed as follows (Irvine 1981, Main and Jones 2002b)

$$m \frac{\partial^2 y_p(x_p, t)}{\partial t^2} = T \frac{\partial^2 y_p(x_p, t)}{\partial x_p^2} \tag{6}$$

where $y_p(x_p, t)$ is the transverse displacement of the cable at point x_p , and x_p is the coordinate along the cable chord axis in the p^{th} segment ($p \leq 2$). To solve Eq. (6) under boundary, continuity and equilibrium conditions, and a distinct solution over the two cable segments is assumed to exist for this the form (Main and Jones 2002b)

$$y_p(x_p, \tau) = Y_p(x_p) e^{\lambda \tau} \tag{7}$$

where the non-dimensional time $\tau = \omega_{01} t$, and $\omega_{01} = \pi / L \sqrt{T/m}$; λ is a dimensionless eigenvalue that is generally complex. λ can be expressed as follows (Main and Jones 2002b)

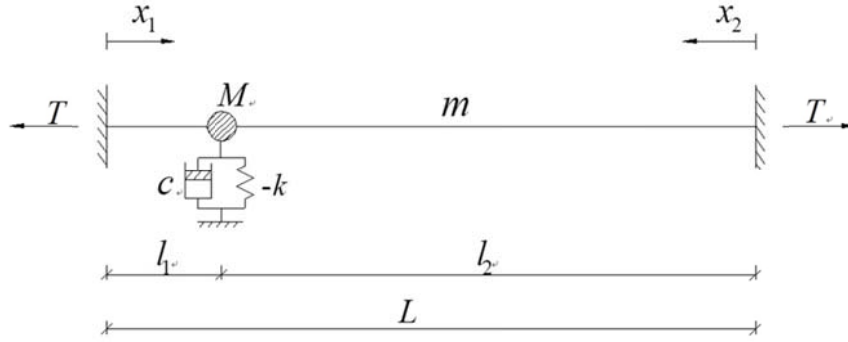


Fig. 11 Taut cable with attached damper, concentrated mass and negative stiffness spring

$$\lambda = \frac{\omega}{\omega_{01}} \left(-\xi + i\sqrt{1-\xi^2} \right) = \alpha + i\beta \tag{8}$$

Where ξ the modal damping ratio, ω is the modulus of the dimensional eigenvalue. β is the non-dimensional frequency and $i = \sqrt{-1}$ is the imaginary unit number.

By substituting Eq. (7) into Eq. (6), the following equation can be obtained

$$\frac{d^2 Y_p(x_p)}{dx_p^2} = \left(\frac{\pi\lambda}{L} \right)^2 Y_p(x_p) \tag{9}$$

Assuming the equation of mode shape (Main and Jones 2002b)

$$Y_p(x_p) = B_p \frac{\sinh(\pi\lambda x_p/L)}{\sinh(\pi\lambda l_p/L)} + C_p \frac{\cosh(\pi\lambda x_p/L)}{\cosh(\pi\lambda l_p/L)} \tag{10}$$

where B_p and C_p are complex parameters, and $\mu_p = \pi l_p/L$ are the non-dimensional cable segment lengths.

The displacement boundary conditions at the cable ends, displacement compatibility equation and the force equilibrium equation at the damper location are

$$y_p(x_p = 0, \tau) = 0, p = 1, 2 \tag{11a}$$

$$y_1(l_1, \tau) = y_2(l_2, \tau) \tag{11b}$$

$$T \left(-\frac{\partial y_1}{\partial x_1} \Big|_{x_1=l_1} - \frac{\partial y_2}{\partial x_2} \Big|_{x_2=l_2} \right) = -k y_1 \Big|_{x_1=l_1} + c \frac{\partial y_1}{\partial t} \Big|_{x_1=l_1} + M \frac{\partial^2 y_1}{\partial x_1^2} \Big|_{x_1=l_1} \tag{11c}$$

By substituting Eq. (7) and Eq. (10) into Eq. (11) the following equations are derived

$$C_1 = C_2 = 0 \tag{12a}$$

$$B_1 + C_1 - B_2 = 0 \tag{12b}$$

$$[-\gamma + \eta\lambda + \phi\lambda^2 + \lambda \coth(\mu_1\lambda)]B_1 + \lambda \coth(\mu_2\lambda)B_2 = 0 \tag{12c}$$

where the non-dimensional mass coefficient is $\phi = \pi M / (mL)$, the non-dimensional damping constant is $\eta = c / \sqrt{Tm}$ and the non-dimensional negative stiffness constant is $-\gamma = -kL / \pi T$.

Eq. (12) can be transformed into matrix form

$$\mathbf{H}\Phi = \mathbf{0} \tag{13}$$

Where \mathbf{H} is the complex matrix

$$\mathbf{H} = \begin{bmatrix} 1 & 1 \\ -\gamma + \eta\lambda + \phi\lambda^2 + \lambda \coth(\Gamma_1) & \lambda \coth(\Gamma_2) \end{bmatrix} \tag{14}$$

where $\Gamma_p = \pi\lambda l_p / L$ and Φ is the corresponding complex vector

$$\Phi = [B_1 \ B_2]^T \tag{15}$$

The infinite set of nontrivial solutions ($\Phi \neq \mathbf{0}$) means that $\det(\mathbf{H})=0$ and the characteristic polynomial is

$$\lambda \sinh(\Gamma) + [-\gamma + \eta\lambda + \phi\lambda^2] \sinh(\Gamma_1) \sinh(\Gamma_2) = 0 \tag{16}$$

4.2 Approximate formulations

When the damper, negative stiffness spring and concentrated mass are near the cable end and the change in the eigenvalue λ induced by the damper, spring and concentrated mass is small, the approximate relationships can be found (Main and Jones 2002b, Zhou *et al.* 2014b) for the damping ratio and non-dimensional frequency

$$\xi_n / (l_1 / L) = E_{mk} \frac{E_{mk} \kappa \pi^2}{1 + (E_{mk} \kappa \pi^2)^2} \tag{17a}$$

$$\beta_n \approx n + \frac{1}{\pi} \frac{\eta^2 \mu_1^3 n^3 - \mu_1^2 n [1 - \mu_1 (\gamma + \phi n^2)] (\gamma + \phi n^2)}{[1 - \mu_1 (\gamma + \phi n^2)]^2 + \eta^2 \mu_1^2 n^2} \tag{17b}$$

where the non-dimensional damper parameter grouping is $\kappa = n \eta l_1 / (L \pi)$, n is the mode number. The factor that considers the effects of the concentrated mass and the negative stiffness spring is:

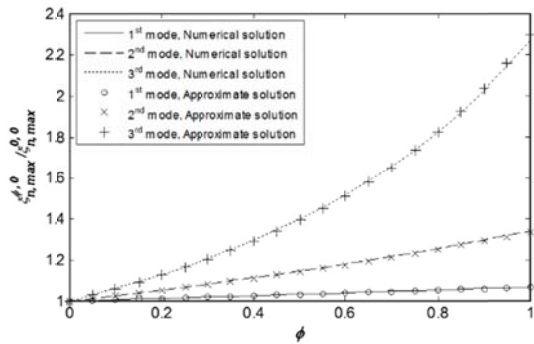
$$E_{mk} = \frac{1}{1 - \mu_1 (\gamma + \phi n^2)} \tag{18}$$

The maximum damping and corresponding non-dimensional damping constant can be derived from Eq. (17a)

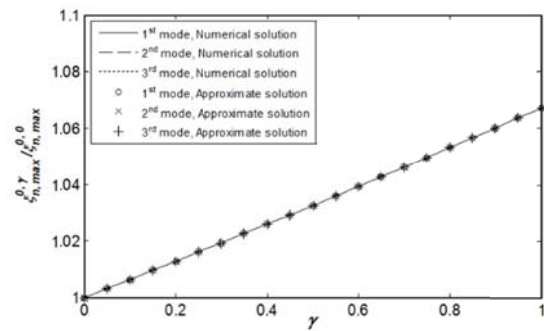
$$\xi_{n,\max} / (l_1/L) = \frac{1}{2} E_{mk} \tag{19}$$

$$\eta_{n,\text{opt}} \cong L / (\pi l_1 n E_{mk}) \tag{20}$$

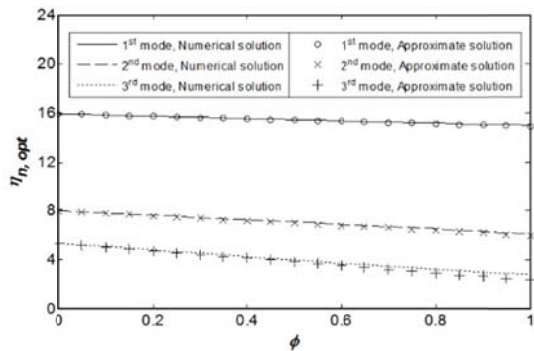
Figs. 12(a) and 12 (b) show a comparison of the numerical and approximate solutions for the maximum damping ratio for the first three modes when the damper position is $l_1/L = 0.02$ and the non-dimensional concentrated mass and negative stiffness coefficient change from 0 to 1, respectively. The ratio $\xi_{n,\max}^{\phi,0} / \xi_{n,\max}^{0,0}$ and $\xi_{n,\max}^{0,\gamma} / \xi_{n,\max}^{0,0}$ can evaluate the effects of ϕ and γ , respectively, where $\xi_{n,\max}^{\phi,0}$ and $\xi_{n,\max}^{0,\gamma}$ are the n^{th} mode maximum damping ratio for different values of ϕ and γ , and $\xi_{n,\max}^{0,0}$ is the maximum damping ratio when $\phi = 0$, $\gamma = 0$ for the n^{th} mode.



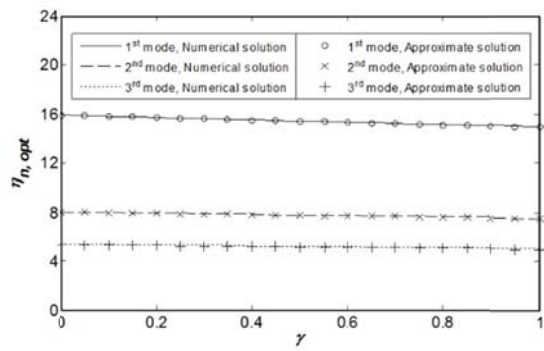
(a) Effects of concentrated mass on maximum damping ratio



(b) Effects of negative stiffness on maximum damping ratio



(c) Effects of concentrated mass on optimum damping constant



(d) Effects of negative stiffness on optimum damping constant

Fig. 12 Maximum damping ratio and optimum damping constant ($l_1/L = 0.02$)

Fig. 12(a) indicates the maximum damping ratio increased in line with the non-dimensional concentrated mass coefficient. The increase in the maximum damping ratio was nonlinear for higher modes of vibration, and the maximum damping ratio of the third mode was much higher than that of the first mode. Fig. 12(b) illustrates that the maximum damping ratio increased when γ increased; however, in contrast to the effects of the non-dimensional concentrated mass coefficient, the maximum damping ratio of the first three modes were almost identical as Eq. (18) shows the effects of non-dimensional negative stiffness is independent from the mode number.

Figs. 12(c) and 12(d) indicated that the non-dimensional optimal damping coefficient corresponding to the maximum damping ratio decreased with an increase in ϕ and γ , respectively. The non-dimensional optimal damping coefficient also decreased when the mode number increased, as Eq. (20) shows the mode number in the denominator.

Figs. 12(a) and 12(b) show $\xi_{n,max}^{\phi,0}$ and $\xi_{n,max}^{0,\gamma}$ increase with increase in ϕ and γ for the first three modes, respectively. The approximate formulation could accurately predict the maximum damping ratio for ϕ and γ when they were smaller than 1.0. Figs. 12(a) and 12(b) also show a distinction that the factor of concentrated mass on maximum damping ratio was multiplied by n^2 as indicated in Eq. (18), while the negative stiffness has no such factor. The difference between the numerical and approximate optimum damper coefficient of the third mode became increasingly obvious as indicated in Fig. 12(c), especially when ϕ approached 1.0.

However, Fig. 12(d) shows the numerical and approximate optimum damper coefficient of the third mode were in good agreement.

4.3 Critical negative stiffness and concentrated mass coefficient

The above show that negative stiffness and concentrated mass could both increase the damping of a taut cable with an attached damper; however, the results are based on an assumption of small frequency change. The critical values of negative stiffness and concentrated mass could be deduced from Eq. (17(b)) when $\eta = 0$

$$\beta_n \approx n - \frac{l_1}{L} \frac{\mu_1(\gamma + \phi n^2)}{1 - \mu_1(\gamma + \phi n^2)} n \tag{21}$$

When the system frequency is reduced to zero, then $\beta_n = 0$ in Eq. (21), and the following Eq. (22) can be derived

$$\gamma_{crit} \approx \frac{L}{L + l_1} \frac{1}{\mu_1} \tag{22a}$$

$$\phi_{crit} \approx \frac{L}{L + l_1} \frac{1}{\mu_1 n^2} \tag{22b}$$

Fig. 13(a) shows the numerical and approximate solutions of the non-dimensional first mode frequency β_1 decreased as γ increased, the approximate formulation could accurately predict the numerical results $\gamma < 10$, it also roughly predicted that β_1 decreased to zero when γ was

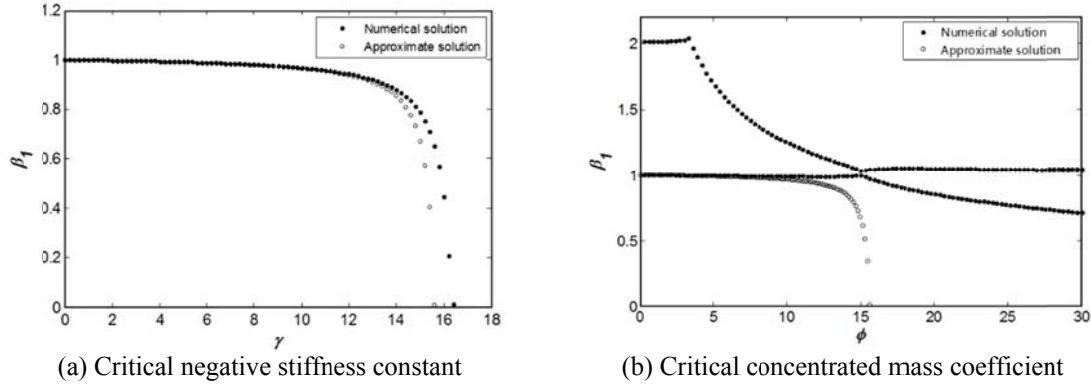


Fig. 13 Non-dimensional first mode frequency with increasing concentrated mass coefficient and negative stiffness constant ($l_1/L = 0.02$)

around 15.6, 16.4, respectively. It should be noted that the frequency of cable with concentrated mass will not reach to zero. Fig. 13(b) shows modal crossover phenomena (Zhou *et al.* 2018) for the first and the second mode when $\eta_{opt} = 6.3$ and $\phi \approx 15.1$ from numerical solution, while the approximate solution (Eq. 22(b)) indicated the critical ϕ was around 15.6. It was found that the Eq. 22(b) could roughly predict this critical ϕ as it corresponding to one solution branch with significant lower damping compared to the other. Anyway, the above shows there are critical negative stiffness and concentrated mass and Eq. (22) can roughly predict the critical value as it was based on the assumption of small frequency shifts.

5. Conclusions

This paper reported tests of full-scale cable with four different types of passive dampers. The logarithmic decrements of the cable with the damper were calculated from the free vibration time histories. The damper efficiency ratio was derived based on the test results. The effects of concentrated mass and negative stiffness on the damping performance were discussed and compared theoretically. It was found that:

- The tested damping of the cable with a damper was always lower than the theoretical damping due to the effects of stiffness. The non-ideal stiffness may introduce from different mechanism: the damper itself due to compression of viscous fluid, air chamber in the damper or supporter flexibility.
- The tested damping of the cable with a non-linear damper was strongly related to the cable vibration amplitude. An extreme example was the cable with friction damper: the highest damping reached the theoretical maximum and the lowest damping was the same as that of the free cable.
- The efficiency ratios of the tested viscous damper, passive-on MR damper, HDR damper were approximately 0.6, 0.6 and 0.3, respectively. The efficiency ratio of the friction damper was between 0–1.0 due to the special working mechanism.

- Negative stiffness and concentrated mass could both increase damper performance. The effects of concentrated mass are different from each mode as the factor contains the square of the mode number, whereas the effects of negative stiffness are independent from the mode number.
- The proposed approximate formula can accurately predict damping behavior when ϕ and γ are smaller than 1.0 for lower mode of vibration. There are critical ϕ and γ values and the proposed equation can roughly predict these values.

Acknowledgments

The authors of this work described in this paper received financial support from the National Natural Science Foundation of China (Grant Nos. 51578336 & 51108269), Shenzhen Knowledge Innovation Plan Project (Grant No. JCYJ20170818102511790) and the Ministry of Science and Technology for the 973-project (No. 2011CB013604), to whom the writers are grateful.

References

- Chen, L., Sun, L.M. and Nagarajaiah, S. (2015), "Cable with discrete negative stiffness device and viscous damper: passive realization and general characteristics", *Smart Struct. Syst.*, **15**(3), 627-643.
- Clough, R.W. and Penzien, J. (2003), *Dynamics of Structures*, (3rd Ed.), *Computers and Structures Inc.* Berkeley, California, USA.
- Hikami, Y. and Shiraishi, N. (1988), "Rain-wind induced vibrations of cables stayed bridges", *J. Wind Eng. Ind. Aerod.*, **29**(1-3), 409-418.
- Irvine, H.M. (1981), *Cable Structures*, MIT Press, Cambridge, Massachusetts, USA.
- Krenk, S. (2000), "Vibrations of a taut Cable with an external damper", *J. Applied Mech.*, **67**(4), 772-776.
- Krenk, S. (2002), "Vibrations of a shallow cable with a viscous damper", *Proceedings Mathematical Physical and Engineering Sciences*, **458**(2018), 339-357.
- Lazar, I.F., Neild, S.A. and Wagg, D.J. (2016), "Vibration suppression of cables using tuned inerter dampers", *Eng. Struct.*, **122**, 62-71.
- Lee, D. and Taylor, D.P. (2001), "viscous damper development and future trends", *Struct. Des. Tall Spec.*, **10**(5), 311-320.
- Lu, L., Duan, Y.F., Spencer, B.F. Jr., Lu, X. and Zhou, Y. (2017), "Inertial mass damper for mitigating cable vibration", *Struct. Control Health Monit.*, **24**: e1986.
- Main, J.A. and Jones, N.P. (2002a), "Analytical Investigation of the Performance of a Damper with a Friction Threshold for Stay-Cable Vibration Suppression", *Proceedings of the 15th ASCE Engineering Mechanics Division Conference*, Columbia University, NY, June.
- Main, J.A. and Jones, N.P. (2002b), "Free vibrations of taut cable with attached damper. I: Linear viscous damper", *J. Eng. Mech.*, **128**(10), 1062-1071.
- Main, J.A. and Jones, N.P. (2002c), "Free vibrations of taut cable with attached damper. II: Nonlinear viscous damper", *J. Eng. Mech.*, **128**(10), 1072-1081.
- Main, J.A. and Jones, N.P. (2007), "Vibration of tensioned beams with intermediate damper. II: Damper near a support", *J. Eng. Mech.*, **133**(4), 379-388.
- Nakamura, A., Kasuga, A. and Arai, H. (1998), "The effects of mechanical dampers on stay cables with high-damping rubber", *Constr. Build. Mater.*, **12**(2-3), 115-123.
- Pacheco, B.M., Fujino, Y. and Sulekh, A. (1993), "Estimation curve for modal damping in stay cables with viscouvdamper", *J. Struct. Eng.*, **119**(6), 1961-1979.
- Shi, X., Zhu, S. and Li, J.Y. (2016), "Dynamic behavior of stay cables with passive negative stiffness

- dampers”, *Smart Mater. Struct.*, **25**(7), 075044.
- Spencer, Jr. B.F., Dyke, S.J., Sain, M.K. and Carlson, J.D. (1997), “Phenomenological model for magnetorheological dampers”, *ASCE J. Eng.Mech.*, **123**(3), 230-238.
- Tabatabai, H. and Mehrabi, A.B. (2000), “Design of Viscous Dampers for Stay Cables”, *ASCE J. Bridge Eng.*, **5**(2), 114-123.
- Xu, Y.L. and Yu, Z. (1998), “Mitigation of three-dimensional vibration of inclined sag cable using discrete oil dampers — II: application”, *J. Sound Vib.*, **214**(4), 675-693.
- Xu, Y.L. and Zhou, H.J. (2007), “Damping cable vibration for a cable-stayed bridge using adjustable fluid dampers”, *J. Sound Vib.*, **306**(2), 349-360.
- Yamaguchi, H. and Fujino, Y. (1998), “Stayed cable dynamics and its vibration control”, *Proceedings of the International Symposium on Advances in Bridge Aerodynamics*, Balkema, Rotterdam, Netherlands, 235-253.
- Zhou, H.J. (2005), “Theory and experimental study on vibration control of stay cables”, Ph.D. Dissertation; Tongji University, Shanghai. (in Chinese).
- Zhou, H.J. and Sun, L.M. (2013), “Damping of stay cable with passive-on magnetorheological dampers: A full-scale test”, *Int. J. Civil Eng.*, **11**(3), 154-159.
- Zhou, H.J., Huang, X.G., Xiang, N., He, J.W., Sun, L.M. and Xing, F. (2018), “Free vibration of a taut cable with a damper and a concentrated mass”, *Struct. Control Health Monit.*, e2251.
- Zhou, H.J., Sun, L.M. and Shi, C. (2006), “A full-scale experimental study on cable vibration mitigation with friction damper”, *J. Tongji Univ.*, **34**(7), 864-868. (in Chinese).
- Zhou, H.J., Sun, L.M. and Xing, F. (2014a), “Damping of full-scale Stay Cable with Viscous Damper: Experiment and Analysis”, *Adv. Struct. Eng.*, **17**(2), 265-274.
- Zhou, H.J., Sun, L.M. and Xing, F. (2014b), “Free vibration of taut cable with a damper and a spring”, *Struct. Control Health Monit.*, **21**(6), 996-1014.
- Zhou, P. and Li, H. (2016), “Modeling and control performance of a negative stiffness damper for suppressing stay cable vibrations”, *Struct. Control Health Monit.*, **23**(4), 764-782.

TY